GEOPHYSICS, VOL. 71, NO. 6 (NOVEMBER-DECEMBER 2006); P. K111–K118, 9 FIGS.
10.1190/1.2356114

Texture-based classification of ground-penetrating radar images

Stephen Moysey[1], Rosemary J. Knight[2], and Harry M. Jol[3]

ABSTRACT

Image texture is one of the key features used for the interpretation of radar facies in ground-penetrating radar (GPR) data. Establishing quantitative measures of texture is therefore a critical step in the effective development of advanced techniques for the interpretation of GPR images. This study presents the first effort to evaluate whether different measures of a GPR image capture the features of the data that, when coupled with a neural network classifier, are able to reproduce a human interpretation. The measures compared in this study are instantaneous amplitude and frequency, as well as the variance, covariance, Fourier-Mellin transform, R-transform, and principle components (PCs) determined for a window of radar data. A 50-MHz GPR section collected over the William River delta in Saskatchewan, Canada, is used for the analysis. We found that measures describing the local spatial structure of the GPR image (i.e., covariance, Fourier-Mellin, R-transform, and PCs) were able to reproduce human interpretations with greater than 93% accuracy. In contrast, classifications based on image variance and the instantaneous attributes agreed with the human interpretation less than 68% of the time. Among the textural measures that preserve spatial structure, we found that the best ones are insensitive to within facies variability while emphasizing differences between facies. For the specific case of the William River delta, the Fourier-Mellin transform, which retains information about the spatial correlation of reflections while remaining insensitive to their orientation, outperformed the other measures. Our work in describing radar texture provides an important first step in defining quantitative criteria that can be used to aid in the classification of radar data.

INTRODUCTION

Ground-penetrating radar (GPR) has the potential to noninvasively investigate geologic heterogeneity at high resolution over large volumes of the subsurface. The interpretation of GPR reflection data, however, is currently highly subjective and based primarily on an interpreter's ability to recognize patterns in a radar image. In particular, differences in reflection amplitude, continuity, configuration, and external form (i.e., the overall shape and extent of a reflection) are key properties that are used to divide an image into distinct units referred to as radar facies (van Overmeeren, 1998). For example, in the radar transect shown in Figure 1, Jol and Smith (1991) identified three dominant radar facies based on the distinctive patterns of reflections observed in the data. Many authors have used reflection patterns in a similar manner to obtain qualitative interpretations of radar facies in GPR data (e.g., Beres and Haeni, 1991; van Heteren et al., 1994; Asprion and Aigner, 1999; Beres et al., 1999). Several studies have demonstrated techniques to quantitatively integrate radar facies into geologic facies models using statistical methods (e.g., Rauber et al., 1998; Regli et al., 2002), though the initial interpretation of the GPR data remained qualitative. While these qualitative studies have been critical for demonstrating the efficacy of the radar facies approach to interpretation, a major advance in the analysis of GPR data will be achieved when quantitative methods of interpretation are developed.

Only recently have researchers begun to investigate methods that quantify the interpretation of GPR reflection data. Corbeanu et al. (2002) used a calibration built between GPR instantaneous attributes (envelope and frequency) and well log data to locate mudstone bodies and estimate the distribution of permeability in a 3D volume of the Ferron Sandstone in Utah. An underlying assumption of their approach was that conditions below the scale of the radar wavelet, e.g., thin-bed tuning effects, were responsible for producing the local variations in the GPR signal that were important for the

Manuscript received by the Editor November 17, 2005; revised manuscript received April 9, 2006; published online October 13, 2006.
[1]Clemson University, School of the Environment, 340 Brackett Hall, Clemson, South Carolina 29634. E-mail: smoysey@clemson.edu.
[2]Stanford University, Department of Geophysics, Mitchell Building 360, 397 Panama Mall, Stanford, California 94305. E-mail: rknight@pangea.stanford.edu.
[3]University of Wisconsin-Eau Claire, Department of Geography, 105 Garfield Avenue, Eau Claire, Wisconsin 54702. E-mail: jolhm@uwec.edu.

interpretation of lithofacies. In contrast, taking an approach analogous to that used in qualitative radar facies analysis, Moysey et al. (2003) used a neural network to discriminate between radar facies based on local patterns of reflections in the data. In this study, the probability of the occurrence of a radar facies at any given location in the subsurface was estimated based on amplitude patterns observed within a 2D moving window passed over a GPR image.

In general, the methods used in the studies of Corbeanu et al. (2002) and Moysey et al. (2003) represent some of the basic strategies (i.e., regression, clustering, and pattern recognition) that can be implemented to quantify the interpretation of radar facies. The relative success of these methods, however, will depend ultimately on the degree to which the information extracted from a GPR data set can characterize individual radar facies and discriminate between different radar facies. It is well known in the field of pattern recognition that the selection of a small number of descriptive features from an image yields far superior classification results compared to classifications based on the full image (Bishop, 1995). As a result, studies that compare the effectiveness of different quantitative measures of a GPR image for interpreting radar facies are urgently needed, though the authors are not aware of any existing studies of this nature. Drawing upon the experience and historical success of the pattern-based approach to interpretation used in qualitative radar facies studies, we suggest that image texture is one of the primary indicators of radar facies in GPR data.

Texture is one of the key properties used by humans to perceive and discriminate between objects (Tuceryan and Jain, 1999). As a result, texture is used often in image analysis applications. In a geophysical context, texture has recently become popular as a tool to assist in the classification of remote sensing data (e.g., Atkinson and Lewis, 2000; Curran, 2001). Gao (2004) built on concepts from the field of image analysis to describe a procedure that compares texture within a seismic data cube to a reference set of texels, thereby producing textural attribute volumes that can aid in seismic facies interpretation. Rea and Knight (1998) and Tercier et al. (2000) used variograms to quantitatively characterize the spatial correlation of amplitude (i.e., reflections) in GPR images. In an analogous fashion, we suggest that image analysis tools could be used as a means to locally quantify textures in radar data.

This paper presents the first known quantitative evaluation of different measures of texture for discriminating between radar facies in GPR reflection data. We have selected the GPR section shown in Figure 1 for our analysis because the radar facies in this image are easily identified visually, thereby allowing human interpretation to act as a reference. Note that the quantitative analysis presented in this study would not be possible if data quality or complexity led to a large degree of uncertainty in the radar facies interpretation of the GPR image. Though we use the artificial neural network classification method described by Moysey et al. (2003), we emphasize that the focus of this work is on comparing the different measures of a GPR image, rather than the specific classification technique. Our analysis provides a first step toward defining quantitative criteria that can be used to optimize the automated classification of radar data.

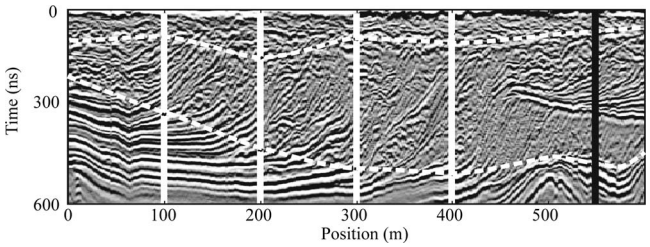

Figure 1. A 50-MHz radar section from William River delta (Jol and Smith, 1991). The interpretation of the section by an expert is illustrated by dashed lines; the facies are uppershore face (top), lower shoreface (middle), and transitional sand and muds (bottom). The vertical lines (white and black) show the location of pseudowells used for training the neural network. The wave velocity reported for the section was 0.07 m/ns and two-way traveltime is shown.

MEASURES OF TEXTURE IN RADAR IMAGES

We define radar texture as a characteristic spatial organization of amplitudes resulting from the GPR imaging process. Broadly defined, however, texture in a gray-scale image describes the spatial variation of the pixel intensities, i.e., grayscale values, within a region of an image (Tuceryan and Jain, 1999). By treating a radar image like a gray-scale image, where the gray-scale value at each pixel corresponds to the reflection amplitude at a given observation time and position in the radar data, we can build on the descriptions of texture that have been developed in the field of image analysis to quantify radar texture.

Texture is inherently a property of areas. Therefore, we define a window of radar data centered on the location x_o,y_o within the radar image $A(x,y)$ as

$$a(x_o,y_o) = A(x,y)\ \forall\ -n_x \le x \le n_x, -n_y \le y \le n_y, \tag{1}$$

where n_x and n_y are half the size of the radar window in each direction covering the rectangular region Ω. The information within the window can be summarized using different transforms of the data that emphasize particular characteristics important for discriminating between radar facies, thereby reducing the potential for misclassification of noisy signals. Many of the transforms we consider are traditional measures of texture used in image analysis problems (i.e., variance, covariance, Fourier-Mellin transform, principle component analysis); others are commonly used in geophysical applications (i.e., instantaneous envelope and frequency); and one we have developed specifically in this work for the analysis of radar reflection data, which we have termed the R-transform.

Transform 1: Variance

Univariate statistics, e.g., the sample variance (S^2) calculated within the window described by equation 1, are common measures used to describe the textural properties of an image (Tuceryan and Jain, 1999):

$$S(x_o,y_o)^2 = \frac{1}{N-1}\sum_{i=-n_x}^{n_x}\sum_{j=-n_y}^{n_y}[a(i,j) - m_a]^2, \tag{2}$$

where m_a and N are the mean and total number of pixels in the window, respectively. Although the variance describes the magnitude of amplitude variations, it does not retain information about the spatial arrangement of values in the window. To demonstrate the loss of discriminatory information, consider the four windows of radar data shown in Figure 2a; each was originally sampled from different regions in the radar image given in Figure 1. The first three windows (A–C) have strong coherent reflections, the key difference between

them being the dip of the reflections. The variance of amplitude within each of these windows is nearly identical, however, making it impossible to discriminate between them. The fourth window (D) does not contain coherent reflections and also has a variance of about half the value of the other three. Therefore, a classification algorithm would be able to discriminate this incoherent sample from the other three, but not based on the obvious geometrical criteria we perceive immediately by looking at the images.

Transform 2: Covariance

A common measure of spatial correlation used in multivariate analysis is the spatial covariance, C(**h**). This quantity provides a measure of the similarity between two points located a distance $|\mathbf{h}| = \sqrt{h_x^2 + h_y^2}$ from each other, where $\mathbf{h} = [h_x, h_y]$ is a lag vector that describes the relative location of two points in the window:

$$C(\mathbf{h}) = \frac{1}{N(h_x,h_y) - 1}\sum_i \sum_j [a(i,j) - m_a][a(i + h_x, j + h_y) - m_a] \; \forall \; i,j,i + h_x, j + h_y \in \Omega. \quad (3)$$

Here, $N(h_x,h_y)$ is the total number of pairs of points in the window that are separated by the vector **h**. In the covariance maps shown in Figure 2b, samples A–D are clearly distinguishable from each other; the direction of maximum correlation is aligned with the direction of dip for windows A–C, and there is no preferential direction of correlation for window D, which is composed of incoherent reflections.

The fact that the spatial covariances are based on relative distances in the window, therefore making them independent of the window's absolute location, is an advantage when classifying radar data because two windows of radar data that have the same pattern of reflections, but are offset by a phase shift, e.g., the windows $a_1 = a(x_o,y_o)$ and $a_2 = a(x_o,y_o + \Delta y)$, could mathematically appear very dissimilar. For example, if a radar image consisted of identical, uniformly spaced flat-lying reflections and if the windows a_1 and a_2 were sampled from the radar image such that Δy was one-quarter of the reflection wavelength, then the reflections in the windows would be out of phase and the mean square difference between the windows would be large, i.e., $\Sigma\Sigma\ (a_1(i,j) - a_2(i,j))^2 \propto S^2$. In practice, when radar facies classifications are performed using amplitude windows, i.e., $a(x,y)$, the decorrelation caused by phase shifts implies that regions with identical textures could be identified as different radar facies. The problem can be avoided, however, when the classification is performed using the covariance of the radar window. Similar conclusions can be made when correlation is used as the measure of similarity between the two windows.

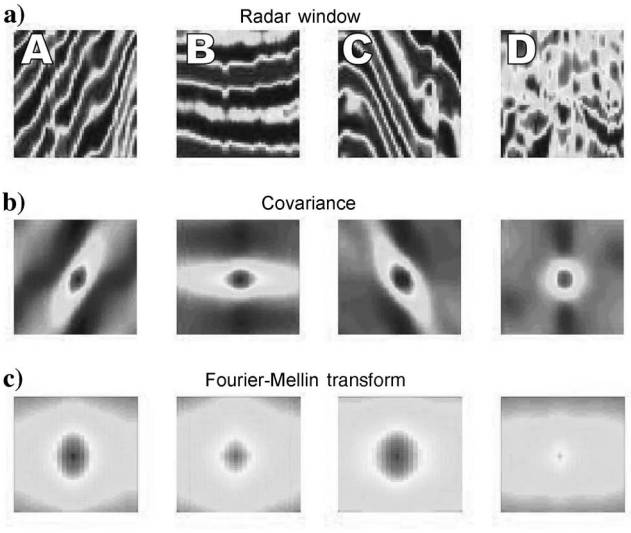

Figure 2. Comparison of statistical measures of texture for four windows of radar data. (a) Windows of radar data sampled from Figure 1. (b) Covariance of radar windows A–D. (c) Fourier-Mellin-based transform of radar windows A–D.

Transform 3: Fourier-Mellin

Although covariance is invariant to translation, it is not invariant to rotation or scaling. If two functions are related by a scaling of the principle Cartesian axes by factors s_x, s_y and through a rotation of angle θ_o, we can write the relationship between them in polar coordinates as

$$f_2(\rho,\theta) = f_1(k\rho, \theta - \theta_o), \quad (4)$$

where $k = \sqrt{s_x^2 \sin^2(\theta - \theta_o) + s_y^2 \cos^2(\theta - \theta_o)}$ is a coefficient that accounts for the scaling factors. Taking the logarithm of the radial axis, we can write both the scaling and rotation as translations in the new coordinate space:

$$f_2(\ln \rho,\theta) = f_1(\ln \rho + \ln k, \theta - \theta_o). \quad (5)$$

The covariance of these functions provides a measure that is invariant to translation in the new log-polar space, which is equivalent to invariance with regard to rotation and scaling in Cartesian coordinates. This is related to what is sometimes referred to as the Fourier-Mellin transform in the literature (e.g., Reddy and Chatterji, 1996; Wood, 1996). If we apply the transform to the covariance of a radar window, we obtain a measure of texture that is invariant to scaling, rotation, and translation. Referring to Figure 2c, we illustrate that the Fourier-Mellin transform of the covariance for radar windows with coherent reflections (A–C) is similar, regardless of reflection orientation. In contrast, the window with chaotic reflection amplitudes (D) has a significantly different transform. We will denote the Fourier-Mellin transform of the covariance of a radar window as $\mathrm{FM}(x,y)$.

Transform 4: R-transform

The next measure of texture has been developed specifically to take advantage of the polarity changes associated with radar wavelets. Because radar data contain both positive and negative polarities, summing along an axis parallel to reflections allows the amplitudes to add constructively (Figure 3), whereas summing over a trajectory perpendicular to the reflections causes the amplitudes of opposite polarity to cancel. Performing the summation for many different angles, we obtain a measure that is sensitive to both the orientation and continuity of reflections in the radar window. Because the summation could be performed over any arbitrary curvilinear trajectory, this measure of texture presents a distinct and powerful conceptual advantage over other measures of reflection continuity, e.g., covariance. In practice, we use the Radon transform $g(\xi,\theta)$ to perform the summation. For an arbitrary function $f(x,y)$, the Radon transform for angle θ is given by

$$g(\xi,\theta) = \int_{-\infty}^{\infty}\int_{-\infty}^{\infty} f(x,y)\,\delta(\xi - x\cos\theta - y\sin\theta)dxdy, \quad (6)$$

where $\delta(-)$ is the Dirac delta function and ξ is the coordinate along the axis perpendicular to the direction of integration (see Bracewell, 2000, for details). To obtain our transform R_a, we next sum along ξ, after squaring the values of the Radon transform to get an overall magnitude of reflection continuity in the direction θ:

$$R_a(\theta) = \int_{-\infty}^{\infty} [g(\xi,\theta)]^2 d\xi. \quad (7)$$

We refer to the quantity given by equation 7 as the R-transform of the radar window $a(x,y)$. Figure 4a presents R_a calculated for each of the four windows of radar data shown in Figure 2a. The R-transform for the 3 samples with coherent reflections (A–C) clearly have peaks at distinct dip angles. In contrast, there is no angle that produces a dominant maximum for the chaotic sample (D). Note that it is possible to derive a form of the R-transform that is sensitive to reflection angle, but not direction, by adding the R-transform to a mirror image of itself:

$$R_a^*(\theta) = R_a(\theta) + R_a(-\theta). \quad (8)$$

The modified version of the R-transform is shown in Figure 4b for each of the four windows of radar data given in Figure 2a. In this case, the modified transform is similar for the two windows with steeply dipping reflections (A and C), but dissimilar for the remaining two windows (B and D).

Transform 5: Principle components analysis (PCA)

The final transform we consider is the projection of the radar windows onto a set of basis images, where each individual basis image, $V_\psi(x,y)$ represents a different type of reflection pattern in the image. The projection of window $a(x_o,y_o)$ onto the ψ basis image in the set is given by

$$PC_\psi(x_o,y_o) = \sum_{i=-n_x}^{n_x}\sum_{j=-n_y}^{n_y} a(i,j)\cdot V_\psi(i,j). \quad (9)$$

We determine the basis images specifically for the radar data under investigation by performing PCA on a set of radar windows sampled from random locations in the radar image, such as those shown in Figure 5. Therefore, in our approach, the set of basis images V_ψ, $\psi = 1,2,\ldots,N_\psi$, are, for a given window size, the N_ψ most significant principle component vectors of the radar image. A good description of PCA in a geologic context is given by Davis (2002).

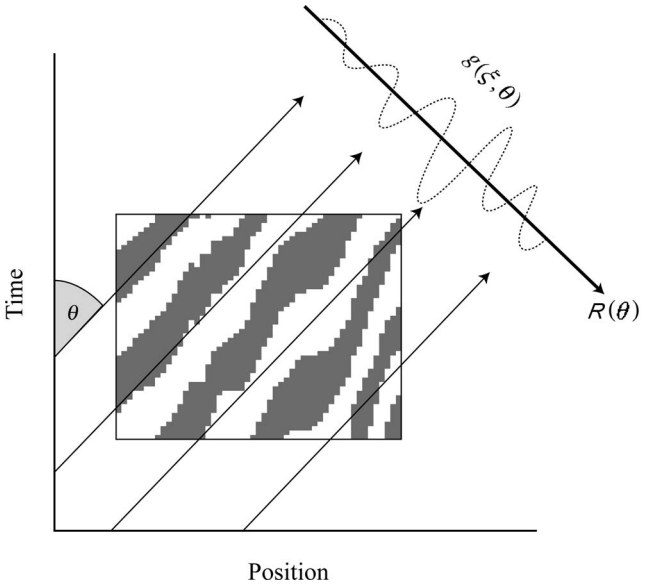

Figure 3. Schematic illustrating the R-transform, $R(\theta)$. The 1D function $g(\xi,\theta)$ is the radon transform of the radar window. The measure $R(\theta)$ used in this paper is the summation of $g(\xi,\theta)^2$ along the ξ axis.

CLASSIFICATION EXAMPLE: WILLIAM RIVER DELTA

We explore radar texture as a discriminator of radar facies for the data set collected from the William River delta, Saskatchewan, Canada, shown in Figure 1. We chose to work with this data because it has several radar facies units with distinctive radar textures that are easily visually distinguishable. The first part of this section describes the geologic setting of the area and the interpretation of the radar data. We then use pseudowells to perform cross-validation tests that quantitatively evaluate the effectiveness of radar texture for radar facies discrimination. Finally, we compare qualitatively the initial interpretation of the radar data to the radar facies maps obtained by neural network classifications using different textural attributes. The comparison allows us to examine the reasons for the success or failure of the automated classification.

Geologic background and radar interpretation

Jol and Smith (1991) describe the William River delta as a 12–18-m-thick, sand-dominated lobate sheet on the southern shore of Lake Athabasca. The sand-rich delta is prograding into the lake over

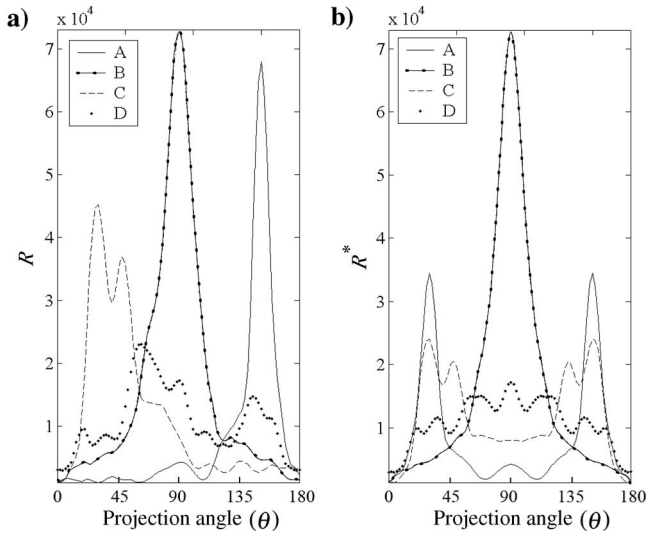

Figure 4. Examples of the R and R* transform obtained for the four sample radar windows shown in Figure 2. Note that R* is only sensitive to the angle of reflector dip, not the dip direction. Angle is in degrees.

lacustrine muds. Three large-scale sedimentary facies make up the internal structure of the delta. Immediately above the mud is a several-meters-thick, transitional facies composed of sands and muds. Above the transitional zone lies a 10–14-m-thick unit of sands with inclined bedding representative of a lower- to middle-shoreface environment. The upper 4–6-m portion of the delta consists of cross-stratified sand, likely related to subaqueous dunes.

The 50-MHz radar image of the William River delta given in Figure 1 shows the facies interpretation by Jol and Smith (1991). Three distinct radar facies were identified in the data: The lower radar facies has horizontally continuous reflections, the middle radar facies is characterized by low-angle inclined reflections, whereas the reflections in the upper facies are discontinuous and wavy. Jol and Smith (1991) used their geologic understanding of lacustrine deltas to establish an associative relationship between these radar facies and the sedimentologic facies described above. A mud diapir identified in the radar image at 500 m and 500 ns was not treated as a separate facies unit in this study because independent data were not available to train the neural network to recognize patterns associated with this type of feature, making it impossible to objectively test our approach.

Classification approach

The method we use for the classification of radar facies is based on the work of Caers and Ma (2002). These authors use feed-forward artificial neural networks to model the probability of facies conditional to observed patterns in seismic data. Moysey et al. (2003) extended the technique for the textural analysis of radar data. Readers are referred to these works for details of the method or to Bishop (1995) for an overview of pattern recognition using neural networks.

In this study, a given measure of texture extracted from a window of radar data is fed to the neural network as an input. The outputs of the network are the probability of occurrence for each of the three radar facies described above. The radar facies with the highest probability is selected as the classification result. Prior to using the neural network for classification, it must be trained first to recognize the relationship between texture and radar facies using a small training data set (e.g., using the information at the pseudowell locations in Figure 1). In this study, we found that the classification accuracy was relatively insensitive to the size of the hidden layer of the neural network used, once a minimum size threshold was achieved; therefore, for all of the examples presented here, we use 25 nodes.

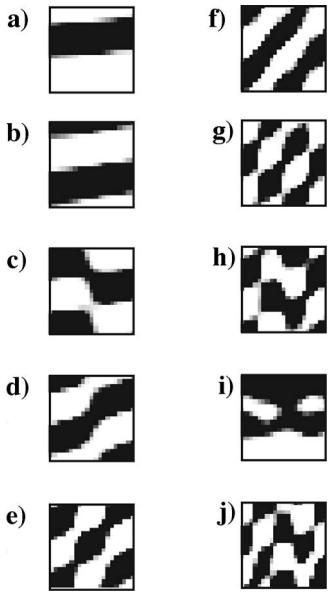

Figure 5. Ten principal components (basis images) determined for the William River delta GPR data using PCA with a 31.5-m × 33.6-ns window (ordered by decreasing significance).

Cross-validation tests

The ability of the neural network to discriminate between radar facies, given a particular measure of texture, was assessed using a cross-validation test. To perform the test, we classified radar facies at one of the pseudowell locations shown in Figure 1 using a neural network that was trained first to recognize the relationship between the radar data and manual interpretation at the other three locations. Assuming that the expert interpretation is true, the classification accuracy is defined as the fraction of locations along the pseudowell where the neural network correctly classified the facies type. The classification accuracy that we report is obtained by averaging the accuracies acquired after repeating the neural network training and classification for each of the four pseudowell locations shown in Figure 1.

Prior to classification, the radar data were processed by applying signal saturation correction, horizontal trace stacking (3 traces), down-trace averaging with a 4.8-ns window, AGC (automatic gain control) using a window of 3 pulse widths, and topographic corrections to produce the radar image shown in Figure 1. These data are gained and therefore no longer represent true reflection amplitudes. However, for large windows, AGC allows relative amplitudes to be preserved locally while balancing amplitudes globally. Therefore reflection patterns, which are the focus of this study, are preserved and enhanced.

Figure 6 shows the classification accuracies obtained for each of the measures of radar texture defined by equations 1–9. For the test, we used a 33.6 ns × 31.5 m (21 × 21 pixel) window of the radar data to calculate the textural attributes. For comparison, we also show the classification accuracy obtained using instantaneous amplitude and frequency, which are defined at points in the image (1.6 ns × 1.5 m), rather than by windows (see Taner et al., 1979).

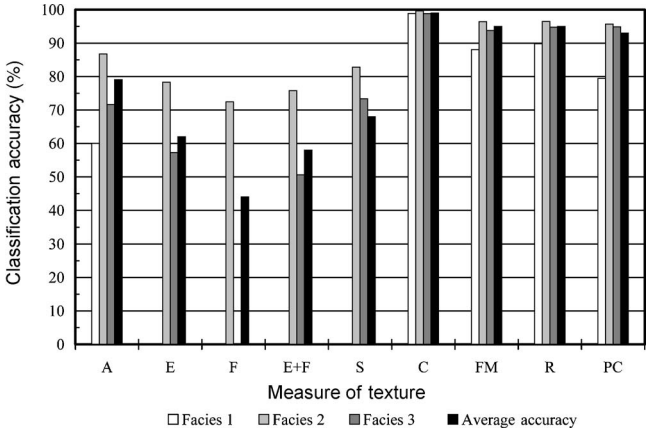

Figure 6. Accuracy of cross-validation tests using different information from the radar image. A — amplitude window, E — instantaneous envelope, F — instantaneous frequency, S — window variance, C — covariance, FM — Fourier-Mellin-based transform, R — R-transform, PC — image basis functions.

Radar facies classification based on windows of the radar data, without any transform, results in an average classification accuracy of 79%, though there is considerable variation in the classification accuracy for each facies (Figure 6). The instantaneous attributes (envelope and frequency) perform poorly ($<65\%$ accuracy). The variance of the radar window was also a relatively poor discriminator of the facies, with a classification accuracy of only 68%. In contrast, the transforms that preserve information about the spatial organization of amplitude variations in the window (i.e., orientation, configuration, continuity, etc.) performed very well — all having a total classification accuracy of over 93%. The transform methods outperform the classification based on the actual radar data window because they emphasize the information used in manually interpreting the data, i.e., texture.

To further investigate how radar texture is represented in the radar image, we repeated the cross-validation test for windows of several different sizes (Figure 7). For these tests, we only compare the results of the radar windows and the covariance of these windows; covariance performed best for the 33.6-ns $\times$ 31.5-m window with a classification accuracy of 99%. The results indicate that a minimum window size of about 25.6 ns $\times$ 24 m is required before the textural properties that define the radar facies are captured. Before this threshold is reached, the classifications based on the window of radar data are superior to those obtained using the covariance transform. Amplitude windows likely produce better classification results initially because it is impossible to obtain statistically meaningful measures of covariance with small data windows. A conceptual limit on the maximum window size occurs when the windows consistently cross facies boundaries, thereby eliminating the generality of the textural pattern. In practice, the training data in our tests included the boundaries between facies; therefore, a decrease in classification accuracy at large window sizes is not observed in Figure 7.

Automated interpretation schemes in the petroleum industry sometimes use trace shape as a criteria for the classification of seismic data (Coléou et al., 2003). Therefore, we also show the radar facies classification results obtained using various 1D windows in Figure 7. In this example, using the textural information available in a 2D window yields more accurate radar facies estimates than can be attained using a 1D window. Additionally, to obtain an equivalent estimation accuracy, the maximum dimension of the window in 2D is much smaller than in 1D, indicating that radar facies estimates can be made at higher resolutions using the 2D window.

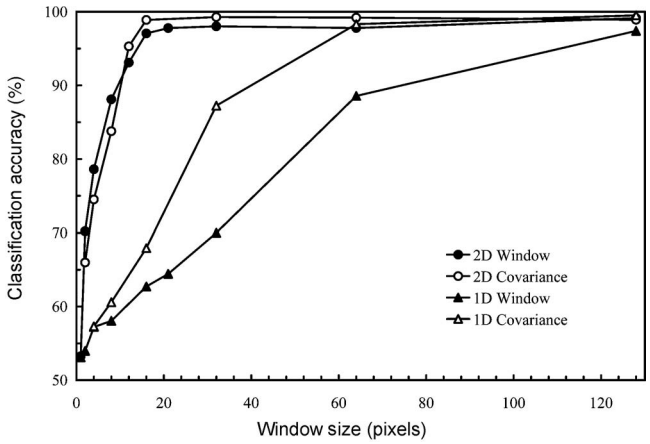

Figure 7. Radar facies classification accuracy as a function of window size. The dimension of a pixel is 1.6 ns $\times$ 1.5 m.

Facies maps

Although the classification accuracy was similar for each of the measures of texture used in the cross-validation tests, it does not mean that the measures are equivalent. Figure 8 shows the facies maps obtained when the entire radar image is classified after training on the four white pseudowells shown in Figure 1. There are key dif-

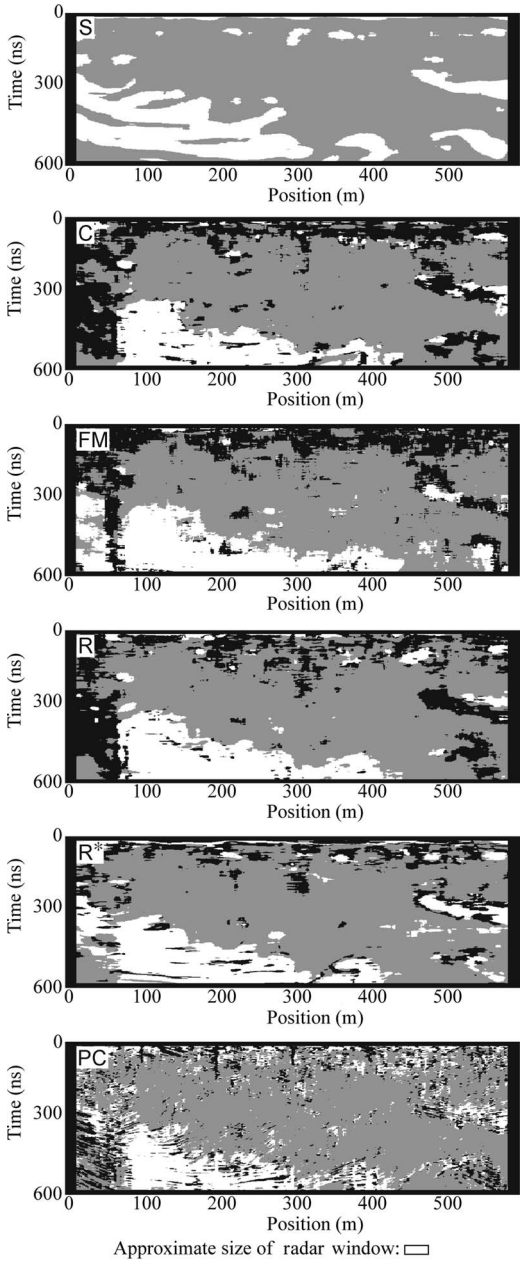

Figure 8. Classification of radar section in Figure 1 using different measures of texture. S — variance, C — covariance, FM — Fourier-Mellin-based transform, R — R-transform, R* — directionally invariant version of the R-transform, PC — image basis functions. The three radar facies described in the text (upper, middle, and lower) are indicated by color (white, gray and black, respectively).

ferences between each of the images. For example, the ability to identify the radar facies located in the top 100 ns of the radar data as a continuous facies unit is significantly different for each measure of radar texture. The wedge on the right-hand side of the radar image, at approximately 300 ns, is also classified differently using the different transforms.

The region of upward-dipping reflections on the bottom left side of the image also provides an interesting example. The measures of texture that are independent of dip direction, i.e., FM and R^*, produce superior classifications of the radar facies in this area. The difference in performance occurs because the data set used to train the neural network, i.e., the locations indicated by the white pseudowells in Figure 1, include only flat-lying reflections or reflections that dip down; the neural network was not trained to associate upward-dipping reflections with the bottom radar facies. Therefore, the neural network fails to produce the correct classification in this region of the radar image when a measure of texture that is sensitive to reflection orientation is used, i.e., C, R, and PC. Expanding the training data by adding a pseudowell that includes upward-dipping reflections in the bottom facies vastly improves the classification result in this area (Figure 9).

The preceding example demonstrates two important points. First, choosing a measure of texture that captures the information needed to discriminate between radar facies, but that remains insensitive to reflection variations within a given facies, can produce better classification results and minimize the size of the training set required. Second, the proper selection of training data, such that it is representative of the entire radar data set to be classified, is a critical problem that must be addressed if acceptable radar facies classification results are to be obtained.

DISCUSSION

In the William River delta example presented above, it is clear that capturing the spatial arrangement of reflections in a GPR image is the key to defining radar facies. The generality of this result is confirmed by the large number of qualitative studies that have cataloged radar facies based solely on the geometric description of reflections in the data, e.g., oblique sigmoidal, subparallel oblique, reflection poor, chaotic, simple layered-parallel, simple layered-wavy, parallel and discontinuous, diffractions, etc. (Beres and Haeni, 1991; van Heteren et al., 1994; Beres et al., 1999; Regli et al., 2002). In a recent review, Neal (2004) presented radar facies as one of the three basic building blocks of radar stratigraphy (the other two were radar surfaces and radar packages). Neal (2004) then built a general catalog of radar facies definitions — similar to those in the studies mentioned above — based on reflection shape, dip, continuity, and the relationship between reflections, i.e., the geometric properties of an image that are captured by the spatial measures of texture presented in this paper (e.g., covariance, Fourier-Mellin, and R-transform).

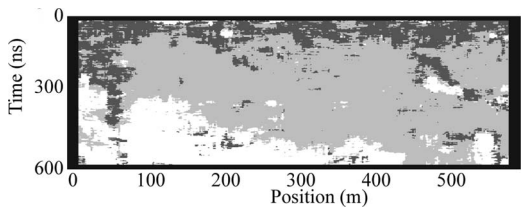

Figure 9. Classification of radar section using covariance after training neural network using both the white and black pseudowells shown in Figure 1.

Although generalizations regarding the definitions of radar facies have been made, it is unlikely that it will be possible to define a universally applicable measure of a radar image. For example, in this study, we found that the characteristics defining the bottom radar facies at the William River delta varied throughout the image. Therefore, it was necessary to select a measure of texture tolerant to variations within each facies, but still able to discriminate between the different facies. Each measure of texture presented in this study emphasizes a different aspect of a radar image. For example, covariance measures the linear continuity of reflections but cannot capture patterns that are more complex. In contrast, the projection of radar windows onto basis images (i.e., as in the PCA approach) can potentially allow very complex spatial patterns to be represented, but these may not generalize well if a large degree of variability is present in the GPR data. Therefore, the measure selected should be tailored to the specific characteristics of the data and needs of the study. The development of adaptive classification methods would help to meet this objective. Likewise, the scale of investigation should be adaptive so that patterns at multiple scales can be analyzed.

Though our study is focused explicitly on radar facies analysis, the ultimate goal of most investigations is to relate GPR data to geology. Many geologic features in the subsurface can produce radar reflections, including boundaries between major lithologic units and small-scale geologic variations related to subfacies structures, e.g., dipping foreset beds in a delta. In this paper, we define lithology to include unconsolidated sediments. Geologic structures produce reflections when the contrasts in lithologic properties associated with them are associated also with changes in electromagnetic properties. For example, the preferential deposition of magnetic minerals (e.g., magnetite) along bedding planes can produce variations in magnetic permeability that could cause radar reflections (e.g., Smith et al., 1999; Moore et al., 2004). However, studies by van Dam and Schlager (2000) and van Dam et al. (2002), suggest that, in most cases, the primary cause of radar reflections is a change in dielectric constant related to spatial variations in water content. One of the key properties that controls the ability of a material to retain water is grain-size distribution. Because grain size is also one of the key properties used to define lithology, it is generally agreed that the reflections observed in a GPR image are primarily related to the lithologic organization of the subsurface (e.g., Neal, 2004).

The link between sedimentary structure and reflections implies that different radar facies represent spatially varying geologic settings in the subsurface. However, Jol and Bristow (2003) caution that many different geologic scenarios can produce similar reflection patterns in a GPR image. Similarly, the dependence of GPR resolution on frequency means that a single depositional environment could produce many different textures (e.g., Huggenberger et al., 1994; Jol, 1995; Jol et al., 2002). Therefore, without additional information or data to provide a geologic context for the field site, the interpretation of geologic facies directly from a GPR image or radar facies interpretation should be avoided.

In general, if radar texture is to be used to characterize radar facies with the ultimate goal of relating radar facies to lithofacies, three criteria must be met. First, geologic regularity that could potentially produce a characteristic reflection pattern in the radar data, e.g., a set of dipping beds, must exist within a lithofacies unit and be distinctive from that in adjacent lithofacies units. Second, the scale of the radar wavelet must be small enough to resolve the internal structure

of a lithofacies to create a distinctive radar texture in a radar image. Finally, complications in the radar data caused by phenomena like multiples, diffractions, and velocity variations cannot be so severe that they obscure the primary reflections originating from lithologic contrasts — subsequent to appropriate processing of the data. An exception to the first two generalities may occur when wave interference between reflections from the top and bottom of a thin bed creates a distinctive, identifiable reflection that is characteristic of that bed (e.g., Cobeanu et al., 2002). We point out that radar units that are defined solely by the arrangement of bounding surfaces cannot be identified using radar texture.

CONCLUSIONS

We have compared six measures of radar texture that can be used to characterize GPR data. When coupled with a classification scheme, such as a neural network, these measures can be used to discriminate between different radar facies, resulting in quantitative radar facies interpretations. Our results suggest that textural measures capturing the spatial arrangement of amplitudes in a GPR image produce radar facies interpretations that are in excellent agreement with those made by human interpreters. In addition, the best correspondence is obtained when the measure of texture used in the classification emphasizes differences between facies, while remaining insensitive to textural variations within facies. Specifically for the case of the William River delta example, the best radar facies classifications were obtained when the measure of texture captured the continuity of reflections in the radar image while remaining insensitive to their orientation (i.e., the Fourier-Mellin and R^*-transforms).

Although our analyses indicate that radar texture can be a powerful criterion for discriminating between radar facies, we note that additional information may be required to assist in radar facies analysis. In particular, finding techniques to identify bounding surfaces in radar data is of the utmost importance to the advancement of automated radar interpretation techniques. Regardless, radar texture will be a useful criterion for the identification of radar facies in many environments. As a result, this work makes an important step in the advancement of automated radar interpretation.

REFERENCES

Asprion, U., and T. Aigner, 1999, Towards realistic aquifer models: three-dimensional georadar surveys of Quaternary gravel deltas (Singen Basin, SW Germany): Sedimentary Geology, **129**, 281–297.

Atkinson, P. M., and P. Lewis, 2000, Geostatistical classification for remote sensing: An introduction: Computers and Geosciences, **26**, 361–371.

Beres, M., and F. P. Haeni, 1991, Application of ground-penetrating-radar methods in hydrogeologic studies: Ground Water, **29**, 375–386.

Beres, M., P. Huggenberger, A. G. Green, and H. Horstmeyer, 1999, Using two- and three-dimensional georadar methods to characterize glaciofluvial architecture: Sedimentary Geology, **129**, 1–24.

Bishop, C. M., 1995, Neural networks for pattern recognition: Oxford University Press.

Bracewell, R. N., 2000, The Fourier transform and its applications: McGraw-Hill Book Company.

Caers, J., and X. Ma, 2002, Modeling conditional distributions of facies from seismic using neural nets: Mathematical Geology, **34**, 139–163.

Coléou, T., M. Poupon, and K. Azbel, 2003, Unsupervised seismic facies classification: A review and comparison of techniques and implementation: The Leading Edge, **22**, 942–953.

Corbeanu, R. M., G. A. McMechan, R. B. Szerbiak, and K. Soegaard, 2002, Prediction of 3-D fluid permeability and mudstone distributions from ground-penetrating radar (GPR) attributes: Examples from the Cretaceous Ferron Sandstone Member, east-central Utah: Geophysics, **67**, 1495–1504.

Curran, P. J., 2001, Remote sensing: Using the spatial domain: Environmental and Ecological Statistics, **8**, 331–344.

Davis, J. C., 2002, Statistics and data analysis in geology: John Wiley and Sons.

Gao, D., 2004, Texture model regression for effective feature discrimination: Application to seismic facies visualization and interpretation: Geophysics, **69**, 958–967.

Huggenburger, P., E. Meier, and M. Beres, 1994, Three-dimensional imaging of fluvial gravel deposits from GPR reflection patterns: A comparison of results of three different antenna frequencies: Fifth International Conference on Ground Penetrating Radar, Waterloo Centre for Groundwater Research, Proceedings, 805–816.

Jol, H. M., 1995, Ground penetrating radar antennae frequencies and transmitter powers compared for penetration depth, resolution and reflection continuity: Geophysical Prospecting, **43**, 693–709.

Jol, H. M., and C. S. Bristow, 2003, GPR in sediments: Advice on data collection, basic processing and interpretation, a good practice guide, *in* C. S. Bristow and H. M. Jol, eds., Ground penetrating radar in sediments: Geological Society of London, 9–27.

Jol, H. M., D. C. Lawton, and D. G. Smith, 2002, Ground penetrating radar: 2-D and 3-D subsurface imaging of a coastal barrier spit, Long Beach, WA, USA: Geomorphology, **53**, 165–181.

Jol, H. M., and D. G. Smith, 1991, Ground penetrating radar of northern lacustrine deltas: Canadian Journal of Earth Sciences, **28**, 1939–1947.

Moore, L. J., H. M. Jol, S. Kruse, S. Vanderburgh, and G. M. Kaminsky, 2004, Annual layers revealed by GPR in the subsurface of a prograding coastal barrier, southwest Washington, USA: Journal of Sedimentary Research, **74**, 690–696.

Moysey, S., J. Caers, R. Knight, and R. M. Allen-King, 2003, Stochastic estimation of facies using ground penetrating radar data: Stochastic Environmental Research and Risk Assessment, **17**, 306–318.

Neal, A., 2004, Ground-penetrating radar and its use in sedimentology: Principles, problems and progress: Earth-Science Reviews, **66**, 261–330, doi: 10.1016/j.earscirev.2004.01.004.

Rauber, M., F. Stauffer, P. Huggenberger, and T. Dracos, 1998, A numerical three-dimensional conditioned/unconditioned stochastic facies type model applied to a remediation well system: Water Resources Research, **34**, 2225–2233.

Rea, J., and R. J. Knight, 1998, Geostatistical analysis of ground-penetrating radar data: A means of describing spatial variation in the subsurface: Water Resources Research, **34**, 329–339.

Reddy, B. S., and B. N. Chatterji, 1996, An FFT-based technique for translation, rotation, and scale-invariant image registration: IEEE Transactions of Image Processing, **5**, 1266–1271.

Regli, C., P. Huggenberger, and M. Rauber, 2002, Interpretation of drill core and georadar data of coarse gravel deposits: Journal of Hydrology, **255**, 234–252.

Smith, D. G., R. A. Meyers, and H. M. Jol, 1999, Sedimentology of an upper-mesotidal (3.7 M) Holocene barrier, Willapa Bay, SW Washington, USA: Journal of Sedimentary Research, **69**, 1290–1296.

Taner, M. T., F. Koehler, and R. E. Sheriff, 1979, Complex seismic trace analysis: Geophysics, **44**, 1041–1063.

Tercier, P., R. J. Knight, and H. M. Jol, 2000, A comparison of the correlation structure in GPR images of deltaic and barrier-spit depositional environments: Geophysics, **65**, 1142–1153.

Tuceryan, M., and A. K. Jain, 1999, Texture analysis, *in* C. H. Chen, L. F. Pau, and P. S. P. Wang, eds., The handbook of pattern recognition and computer vision: World Scientific Publishing, 207–248.

van Dam, R. L., and W. Schlager, 2000, Identifying causes of ground-penetrating radar reflections using time-domain reflectometry and sedimentological analyses: Sedimentology, **47**, 435–449.

van Dam, R. L., and W. Schlager, M. J. Dekkers, and J. A. Huisman, 2002, Iron oxides as a cause of GPR reflections: Geophysics, **67**, 536–545.

van Heteren, S., D. M. FitzGerald, and P. A. McKinlay, 1994, Application of ground penetrating radar in coastal stratigraphic studies: Fifth International Conference on Ground Penetrating Radar, Waterloo Centre for Groundwater Research, Proceedings, 869–881.

van Overmeeren, R. A., 1998, Radar facies of unconsolidated sediments in The Netherlands: A radar stratigraphy interpretation method for hydrogeology: Journal of Applied Geophysics, **40**, 1–18.

Wood, J., 1996, Invariant pattern recognition: A review: Pattern Recognition, **29**, 1–17.